Robust MISO coherent optical GEO satellite feeder link with relaxed implementation constraints

Youssef Minyari
Lab-STICC UMR 6285
IMT Atlantique / TéSA
Brest, France
youssef.minyari@imt-atlantique.fr

Aubin Lecointre
Research Technology and Product Dept.
Thales Alenia Space
Toulouse, France
aubin.lecointre@thalesaleniaspace.com

Raphaël Le Bidan
Lab-STICC UMR 6285
IMT Atlantique, MEE Dept.
Brest, France
raphael.lebidan@imt-atlantique.fr

Charly Poulliat
IRIT UMR 5505
Toulouse INP - ENSEEIHT
Toulouse, France
charly.poulliat@enseeiht.fr

***Abstract*—In this paper, we propose to study the potential advantages that multiple-input single-output (MISO) architectures could offer compared to the classical single-input single-output (SISO) approach for coherent free space optical (FSO) ground-to-GEO feeder links, highlighting their resilience to atmospheric turbulence and the benefits of spatial diversity. Evaluating system trade-offs under both power-limited and power-augmented scenarios, we demonstrate that MISO designs can achieve higher data rates and enable more robust optical feeder links. Choosing the best MISO configuration depends on system-level priorities, including available transmit power, optical and adaptive optics (AO) complexity, throughput-latency balance, and integration requirements. Our findings demonstrate that simple MISO architectures can effectively balance aperture size, AO requirements, interleaver depth, and transmit power, positioning them as a promising solution for efficient and resilient GEO optical feeder links.**

Keywords—Atmospheric turbulence, free space optical communication, GEO uplink, coherent detection, MISO, diversity.

I. INTRODUCTION

Nowadays, satellite telecommunications is a major business with commercial civilian, institutional and governmental use cases. The challenge for space players is to provide ever-higher data rates, greater security and global connectivity, in order to serve Earth areas without Internet access, relay high-resolution images from observation satellites or provide secure links between ground stations and government satellites. In this context, GEO free-space optical (FSO) links are emerging as a promising solution to meet the growing demand for bandwidth and improve the quality of services, while reducing the size and the cost of the communication system. Free-space optical links confer significant advantages over the traditional radio frequency (RF) solutions such as increased bandwidth, license-free access, high directivity, robustness against interception and jamming as well as terminal compactness [1], [2]. Nevertheless, optical communication links still suffer from the need for site diversity to overcome the cloud obstruction, the limited maturity of components suited for space environment, the need for complex pointing systems, and the optical signal distortions resulting from atmospheric propagation. One primary technological limitation of receivers in ground-to-GEO scenario is their susceptibility to atmospheric turbulence [3]. The latter may induce long, deep received optical power fades that can lead to significant performance degradation, including link outages and reduced data rates.

On-orbit GEO optical feeder demonstrations have so far focused on direct detection (IM/DD), leveraging intensity modulation with relatively simple receivers. Reported throughputs have reached the multi gigabit-per-second range [4], [5]. While IM/DD is attractive for its hardware simplicity and ease of implementation, its spectral efficiency and ability to exploit multiplexing are fundamentally limited. Coherent detection, in contrast, can drastically increase capacity up to terabit-per-second [6] by enabling higher-order PSK/QAM modulation formats, polarization multiplexing, and more efficient wavelength-division multiplexing (WDM). However, realizing such coherent GEO links places more stringent requirements on optical and control subsystems, including narrow-linewidth lasers and local oscillators (LO), high-speed DSP chains, high-power optical amplifiers (HPOA), and high-precision pointing, acquisition and tracking (PAT) subsystems.

Within coherent architectures, most if not all of the dual-polarization QPSK (DP-QPSK) Single Input Single Output (SISO) GEO feeder systems currently under study handle deep fades through the combination of high optical power amplifiers, large aperture telescopes with complex adaptive optics (AO), and deep interleaving. These factors help to achieve viable GEO feeder optical link budget and to confirm optical link as a promising solution. However, all these technological enablers raise the size, weight, power and cost of the system. This gap between the capacity promise and the practical challenges faced by SISO architectures motivates the present work. In parallel, coherent optical techniques have been demonstrated in space for inter-satellite and LEO-to-ground links using a homodyne BPSK architecture [7], but not yet in operational GEO feeder scenarios.

This paper explores a slightly different route to address the aforementioned challenges, by considering the alternative or complementary use of multiple-input multiple-output (MIMO) technologies in DP-QPSK GEO feeder links. Specifically, we choose to focus on a 2×1 multiple-input single-output (MISO) Alamouti system [8] for its low hardware decoding cost, afforded by the orthogonality of the coding scheme. Published MIMO FSO demonstrations using either direct detection (IM/DD) or coherent detection are limited to horizontal outdoor links over only a few kilometers [5], [9]–[12], negligible relative to GEO feeder link distances. To the best of our knowledge, their applicability to coherent GEO feeder links has not yet been established. The present study aims to quantify the achievable gains in architectures with multi-transmit-aperture GEO feeder uplinks in the presence of atmospheric turbulence. We adopt SISO DP-QPSK as the reference coherent architecture that is widely adopted in GEO coherent FSO feeder link studies. The driving question is whether the spatial diversity can help relax some of the implementation challenges faced by SISO systems due to the atmospheric turbulence deep fades (extreme HPOA levels, very large apertures with complex AO, deep

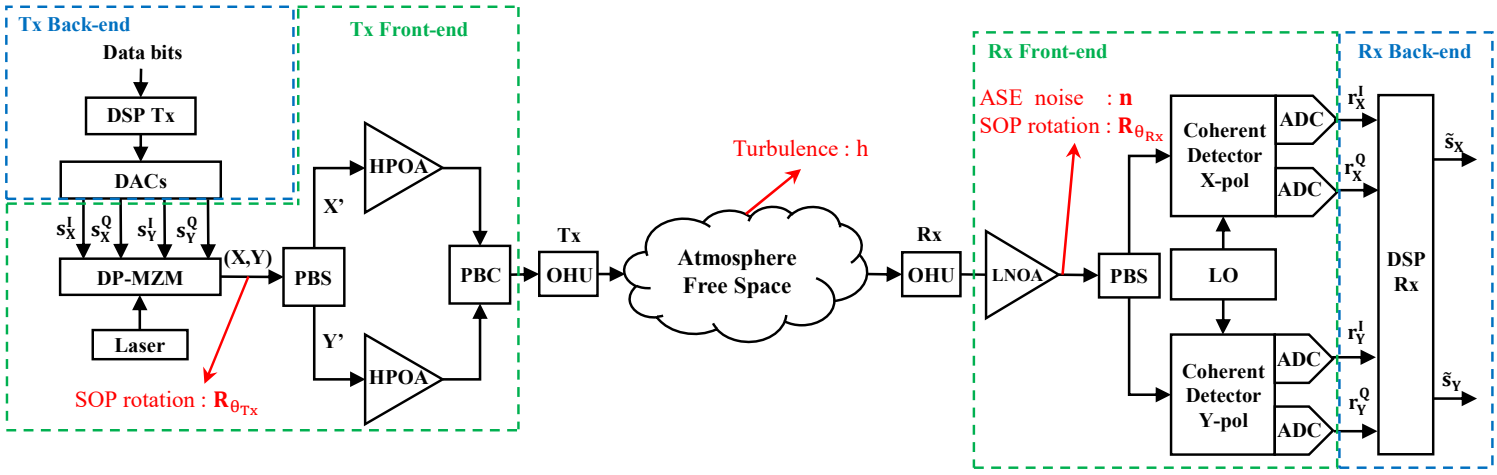

Fig. 1. SISO Tx/Rx Architecture

interleaving…) while improving link robustness and efficiency, so as to make this approach worth the extra cost.

This paper is organized as follows: Section II describes the SISO architecture, key challenges, and simplified channel model. Section III introduces the MISO 2×1 configurations and their challenges. Section IV presents the realistic atmospheric turbulence time-series used in this study and the method used to extend them to longer durations. Section V presents and discusses the results. Finally, Section VI gives concluding considerations.

II. SISO System: Architecture and Channel Model

A. SISO System Architecture

In this study, we adopt the reference uplink SISO architecture developed by Thales Alenia Space under the programs VERTIGO [13] with the European Union (EU) and COOP (COmmunications OPtiques) with the French Space Agency (CNES). The SISO baseline operates at 1550 nm and uses two orthogonal linear polarizations (X and Y) with DP-QPSK at a symbol rate of 56 GBd per polarization. The ground segment employs a single transmit aperture with adaptive optics (AO) and mono-polarization high-power optical amplification, while the receiver uses one single aperture and performs coherent detection. To meet availability targets under turbulence-induced fades, the uplink baseline includes forward-error correction (FEC) with interleaving. This SISO configuration serves as the conventional benchmark for comparison with the proposed MISO approaches presented in this paper.

As depicted in Fig. 1, the ground and space segments are composed of the following parts:

- Ground Transmitter (Tx) :
  - **Tx Back-end:** interfaces with the on-ground computer (OGC) and Tx Front-End. It formats the transmitted bits and generates the electrical signals of the in-phase (I) and quadrature (Q) channels for each polarization.
  - **Tx Front-end:** interfaces with Tx Back-end and the optical head unit (OHU). It performs the electrical-to-optical conversion of the transmitted signal.
- On-Board Receiver (Rx) :
  - **Rx Front-end:** interfaces with Rx Back-End and the optical head unit (OHU). It converts the received optical signal into electrical signals corresponding the I/Q channel for each polarization.
  - **Rx Back-end:** interfaces with Rx Front-End and the digital transparent processor or the on board processor. It uses Digital Signal Processing algorithms to correct the impairments and demodulate the received DP-QPSK signal.

B. SISO Design Challenges

The effect of atmospheric turbulence is more severe on the uplink [3]. For this reason, we limit our study to the ground-to-GEO, as it provides the worst-case scenario for coherent SISO GEO feeder links. From a system-level point of view, uplink design faces several challenges due the current limitations in the technologies involved:

- **Interleaving depth:** Ideally, one would want the deepest interleaving possible to mitigate the effects of turbulence-induced fades. Given the optical channel coherence time (0.1-10ms [1]) and target symbol rate per polarization (56 GBd), this implies buffering millions of symbols which requires enormous and very costly High Bandwidth Memory (HBM). In practice, a smaller interleaver is preferable. Ideally, the memory should be integrated into the chip to overcome these limitations [14].
- **Telescope size:** A larger telescope would help mitigate large path loss and scintillation [15]. However, the size of the telescope is limited by constraints related to cost, weight and volume. Therefore, finding an optimal balance between performance and practical constraints is crucial.
- **Adaptive Optics (AO):** AO systems play a critical role in mitigating the detrimental effects of atmospheric turbulence by correcting the wavefront distortions. However, as the diameter of the aperture increases, the adaptive optics system must become more sophisticated. This leads to increased system cost, volume, and weight, presenting further engineering challenges in the pursuit of higher-performance optical links.
- **High Power Optical Amplifiers (HPOA):** The HPOA developed for terrestrial use do not provide the amplification required for a GEO cross-atmospheric link. This necessitates the development of specific

components and the amplification of the X and Y polarizations separately in the architecture of COOP project (Fig. 1). This approach increases costs (requiring two amplifiers instead of one), and potentially introduces other issues, such as imbalances or skew.

For a high-level system design comparison with the MISO system that will be introduced later on, a simplified channel model capturing only certain key selected transmission impairments is adopted and described in the next subsection.

C. Simplified Channel Model

Let $\mathbf{s} = \begin{pmatrix} s_X \\ s_Y \end{pmatrix}$ be the dual-polarization discrete-time DP-QPSK symbol vector at a given symbol interval, where for Pol$\in\{X, Y\}$ we write $s_{Pol} = s_{Pol}^{I} + js_{Pol}^{Q}$; the superscripts I and Q denote the in-phase and quadrature components of the signal. For simplicity of notation, the time index will be introduced when needed.

In dual-polarization systems, various impairments can affect the transmitted signals. Among these, State Of Polarization (SOP) rotation is particularly important because it directly induces mixing between the X and Y polarization components, which can degrade overall system performance. Therefore, we focus on this impairment in our study. For the purpose of high-level system comparison, we model only three primary transmission impairments in the channel: SOP rotation, additive spontaneous emission (ASE) noise (representing hardware and optical fiber impairments), and dynamic turbulent-induced fluctuations:

- **State of polarization (SOP) rotation:** in our system, SOP rotation arises mainly from propagating through successive media and components such as Mach-Zehnder modulators (MZMs), single mode fiber (SMF), and HPOA. The resulting SOP rotation is modelled as a real 2×2 rotation matrix:

$$\mathbf{R}_\theta = \begin{pmatrix} \cos(\theta) & -\sin(\theta) \\ \sin(\theta) & \cos(\theta) \end{pmatrix}$$

  Atmospheric turbulence effect on the SOP rotation can be neglected in the case of linear polarizations compared to the optical fiber effect [16].
- **Amplified Spontaneous Emission (ASE) noise:** induced mainly by optical amplifiers: HPOA at the transmitter low noise optical amplifier (LNOA) at the receiver. It is widely modeled as an additive white Gaussian noise with a total power per polarization of:

$$N_0 = Nhf(G - 1)B_0$$

  where N is the noise factor, *h* the Planck's constant, f the frequency, G the amplifier gain, and B_0 the reference bandwidth. For our DP-QPSK system, the dual-polarization noise vector is modeled as $\mathbf{n} = \begin{pmatrix} n_X \\ n_Y \end{pmatrix}$, where for Pol $\in\{X, Y\}$, $n_{Pol} \sim \mathcal{CN}(0, N_0)$.
- **Atmospheric turbulence:** in this study, we consider that it affects both polarizations X and Y similarly in both amplitude and phase and without intra-polarization effects [17]. Therefore, the atmospheric turbulence is a diagonal matrix given by $\mathbf{H} = h\mathbf{I}_2$, where $\mathbf{I}_2$ is the 2×2 identity matrix, and $h \in \mathbb{C}$ is the induced turbulence amplitude and phase fluctuations multiplying both polarizations of the system. Turbulence statistics will be modeled using realistic time-series for the channel fading coefficients, as will be described in section IV.

Static losses either in components (e.g., insertion and coupling losses) or in the free space (atmospheric scattering and absorption, cloud and propagation losses) are included in the static link budget that sets the received optical power (ROP). All other synchronization and hardware impairments (e.g. timing/frequency offsets, I/Q imbalance, phase noise and pointing errors, etc.) are assumed to be perfectly compensated by the coherent digital receiver, and thus are not modeled. Considering the simplified channel described previously, the received dual-polarization discrete-time signal can be written as follows:

$$\begin{aligned} \mathbf{r} &= \begin{pmatrix} r_X^I + jr_X^Q \\ r_Y^I + jr_Y^Q \end{pmatrix} \\ &= \mathbf{R}_{\theta_{Rx}} \mathbf{H} \mathbf{R}_{\theta_{Tx}} \mathbf{s} + \mathbf{n} \\ &= h\mathbf{R}_{\theta_{tot}} \mathbf{s} + \mathbf{n} \end{aligned} \quad (1)$$

where $\mathbf{R}_{\theta_{tot}} = \mathbf{R}_{\theta_{Rx}} \mathbf{R}_{\theta_{Tx}} = \mathbf{R}_{\theta_{Rx}+\theta_{Tx}}$, θ_{Tx} and θ_{Rx} are the SOP rotation angles sat the transmitter and at the receiver respectively.

The rotation of X-Y axis in (1) can be corrected by channel estimation using pilots, or alternatively in a non-data-aided manner with a blind equalizer such as Constant Modulus Algorithm (CMA) [18]. After equalization, each polarization of the received signal can be demodulated separately. Controlling the state of polarization is crucial in DP-QPSK systems to ensure proper demodulation. Let us now introduce the modifications that arise in the transmit architecture and channel model when replacing the SISO system with a MISO system.

III. MISO 2×1 System Design

This section presents a dual-polarization 2×1 MISO uplink employing Alamouti-based diversity technique. The section is divided into three subsections: A describes the transmitter/receiver architectures. B discusses two possible implementations of Alamouti 2×1 coding schemes, and C presents the challenges of the MISO system.

A. MISO System Architecture

The MISO Alamouti 2×1 system under consideration employs two ground transmitters and one on-board coherent receiver (Fig. 2). The ground transmitters are spaced by more than the atmospheric coherence length (Fried parameter r_0) typically on the order of 5-30cm depending on the turbulence strength [3].

In our system, transmit branches can be implemented either as two distinct telescopes, hence two OHUs, as shown in Fig. 2 or as a single telescope with two apertures. In both cases, each transmit branch replicates the full dual-polarization Tx Front-end. The Tx Back-end performs the Alamouti coding, which guarantees the diversity gain and improves the system's robustness to atmospheric turbulence, as we will show in section V. Both beams are transmitted simultaneously and are time-aligned at the receiver; differential delays are considered perfectly compensated. The Rx Front-end remains identical to the SISO case; on-board

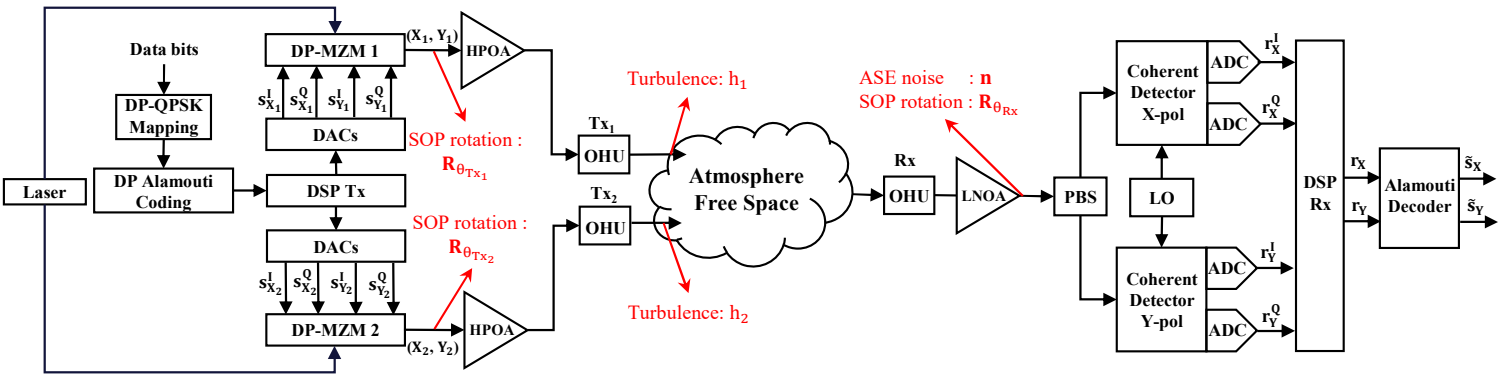

Fig. 4. MISO 2×1 Tx/Rx Architecture

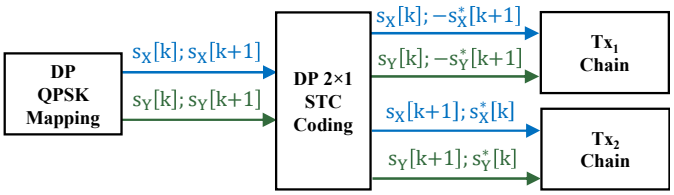

Fig. 3. MISO 2×1 STC Coding over two consecutive symbol intervals for X-pol (blue arrows) and Y-pol (green arrows)

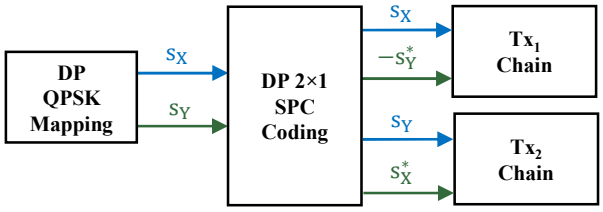

Fig. 2. MISO 2×1 SPC Coding over one symbol interval for X-pol (blue arrows) and Y-pol (green arrows)

costs are unchanged. In the Rx Back-end, the DSP performs Alamouti decoding to recover the transmitted signal.

As the ground station has four degrees of freedom (2 transmitters and 2 polarizations), DP Alamouti Coding stage in Fig. 2 can be implemented by exploiting space and time dimensions (space-time coding, STC)) or by exploiting space and polarization dimensions (space-polarization coding, SPC). These two implementations are presented next.

B. STC and SPC Schemes

This subsection introduces two possible Alamouti coding schemes. As the transmitters are assumed to be spaced apart by a distance greater than the coherence length, the turbulent channels experienced by each transmitter are assumed uncorrelated. To check that the performance of these two schemes are the same, we adapted the previous discrete-time channel model and considered a channel with only ASE and atmospheric turbulence.

1) Space-Time Coding (STC)

As illustrated in Fig. 3, the proposed STC applies the classical Alamouti coding [8] on each polarization. For each polarization Pol ∈ {X, Y}, we note $s_{Pol}[k]$ and $s_{Pol}[k+1]$ two T_s-spaced consecutive symbols, T_s being the symbol period. The received signal $\mathbf{r}_{STC}$ over two consecutive symbol periods, expressed in 2×2 matrix form:

$$\begin{aligned}\mathbf{r}_{STC} &= \begin{pmatrix} r_X[k] & r_X[k+1] \\ r_Y[k] & r_Y[k+1] \end{pmatrix} \\ &= h_1 \begin{pmatrix} s_X[k] & -s_X^*[k+1] \\ s_Y[k] & -s_Y^*[k+1] \end{pmatrix} + h_2 \begin{pmatrix} s_X[k+1] & s_X^*[k] \\ s_Y[k+1] & s_Y^*[k] \end{pmatrix} \\ &\quad + \begin{pmatrix} n_X[k] & n_X[k+1] \\ n_Y[k] & n_Y[k+1] \end{pmatrix} \end{aligned} \quad (2)$$

where the superscript (*) denotes the complex conjugate and h_i is the complex channel coefficient of the transmitter i.

In this case, the system is equivalent to two independent STC Alamouti 2×1 schemes (one per polarization). Therefore, to recover the decoded symbols noted $\tilde{s}_{Pol}$, the classical Alamouti decoding applied to (2) is performed per polarization Pol ∈ {X, Y} following these equations:

$$\begin{cases} \tilde{s}_{Pol}[k] = h_1^* r_{Pol}[k] + h_2 r_{Pol}^*[k+1] \\ \qquad\quad = (|h_1|^2 + |h_2|^2) s_{Pol}[k] + \bar{n}_{Pol}[k] \\ \tilde{s}_{Pol}[k+1] = h_2^* r_{Pol}[k] - h_1 r_{Pol}^*[k+1] \\ \qquad\quad = (|h_1|^2 + |h_2|^2) s_{Pol}[k+1] + \bar{n}_{Pol}[k+1] \end{cases} \quad (3)$$

2) Space-Polarization Coding (SPC)

As illustrated in Fig. 4, the SPC coding is performed over one symbol time-slot: symbols are transmitted over the X-polarization and the conjugates over Y-polarization. The received signal $\mathbf{r}_{SPC}$ over one symbol period can be written as follows:

$$\begin{aligned}\mathbf{r}_{SPC} &= \begin{pmatrix} r_X[k] \\ r_Y[k] \end{pmatrix} \\ &= h_1 \begin{pmatrix} s_X[k] \\ -s_Y^*[k] \end{pmatrix} + h_2 \begin{pmatrix} s_Y[k] \\ s_X^*[k] \end{pmatrix} + \begin{pmatrix} n_X[k] \\ n_Y[k] \end{pmatrix} \end{aligned} \quad (4)$$

Decoding (4) can be performed jointly between the two polarizations in the same time-slot using the following Alamouti decoding equations:

$$\begin{cases} \tilde{s}_X[k] = h_1^* r_X[k] + h_2 r_Y^*[k] \\ \qquad = (|h_1|^2 + |h_2|^2) s_X[k] + \bar{n}_X[k] \\ \tilde{s}_Y[k] = h_2^* r_X[k] - h_1 r_Y^*[k] \\ \qquad = (|h_1|^2 + |h_2|^2) s_Y[k] + \bar{n}_Y[k] \end{cases} \quad (5)$$

Equations (3) and (5) show that both schemes reach the same diversity. However, the difference between these two configurations is the decoding delay: SPC requires only one symbol time while STC requires two. Therefore, SPC scheme seems more appropriate for a practical implementation.

C. MISO Technical Challenges and Cost

Compared to a SISO system, the MISO system duplicates most of the transmit chain which comes with additional costs and sources of impairments related to phase mismatch, timing misalignment and amplitude imbalance. These impairments will not be considered in the present study and deserve dedicated investigation but are not foreseen as a critical limitation. A more serious concern is raised by the sensitivity of the considered Alamouti coding schemes to the SOP mismatch at the transmitter side, as explained below.

In the general case, as shown in Fig. 2, each transmitter can experience a different SOP rotation. To assess the impact of this impairment on decoding quality, we examine its effect on the STC scheme. The received signal in the STC configuration becomes:

$$\begin{aligned}\mathbf{r}_{\mathrm{STC}} &= \begin{pmatrix} r_X[k] & r_X[k+1] \\ r_Y[k] & r_Y[k+1] \end{pmatrix} \\ &= h_1 \mathbf{R}_{\theta_1} \begin{pmatrix} s_X[k] & -s_X^*[k+1] \\ s_Y[k] & -s_Y^*[k+1] \end{pmatrix} + \\ &\quad h_2 \mathbf{R}_{\theta_2} \begin{pmatrix} s_X[k+1] & s_X^*[k] \\ s_Y[k+1] & s_Y^*[k] \end{pmatrix} + \begin{pmatrix} n_X[k] & n_X[k+1] \\ n_Y[k] & n_Y[k+1] \end{pmatrix} \end{aligned} \quad (6)$$

where $\mathbf{R}_{\theta_i} = \mathbf{R}_{\theta_{Rx}+\theta_{Tx_i}}$ is the total rotation matrix and θ_{Tx_i} is the rotation angle at transmitter i.

In order to verify the effective power gain achieved by the STC coding scheme under uncontrolled SOP rotations at the transmitters, we rewrite the received signal $\mathbf{r}_{\mathrm{STC}}$ in a vector form to expose explicitly the transmitted symbols, starting from (6), as follows:

$$\begin{aligned}\mathbf{r}'_{\mathrm{STC}} &= \begin{pmatrix} r_X[k] \\ r_Y[k] \\ r_X^*[k+1] \\ r_Y^*[k+1] \end{pmatrix} \\ &= \begin{pmatrix} h_1 \mathbf{R}_{\theta_1} & h_2 \mathbf{R}_{\theta_2} \\ h_2^* \mathbf{R}_{\boldsymbol{\theta_2}} & -h_1^* \mathbf{R}_{\theta_1} \end{pmatrix} \begin{pmatrix} s_X[k] \\ s_Y[k] \\ s_X[k+1] \\ s_Y[k+1] \end{pmatrix} + \begin{pmatrix} n_X[k] \\ n_Y[k] \\ n_X^*[k+1] \\ n_Y^*[k+1] \end{pmatrix} \\ &= \mathbf{H}_{\mathrm{STC}} \mathbf{s} + \mathbf{n} \end{aligned} \quad (7)$$

As explained in [19, Sec. 7.1.2], the power gain of the MISO scheme can be evaluated by examining the singular values of the equivalent channel matrix $\mathbf{H}_{\mathrm{STC}}$, i.e., the square root of the eigenvalues of:

$$\mathbf{H}_{\mathrm{STC}}^{\dagger} \mathbf{H}_{\mathrm{STC}} = \begin{pmatrix} (|h_1|^2 + |h_2|^2)\mathbf{I}_2 & \mathbf{A} \\ \mathbf{A}^{\dagger} & (|h_1|^2 + |h_2|^2)\mathbf{I}_2 \end{pmatrix} \quad (8)$$

where the superscript (†) denotes the conjugate transpose, $\Delta\theta = \theta_1 - \theta_2$, and $\mathbf{A} = 2h_1^* h_2 \sin(\Delta\theta) \begin{pmatrix} 0 & 1 \\ -1 & 0 \end{pmatrix}$.

The eigenvalues of $\mathbf{H}_{\mathrm{STC}}^{\dagger}\mathbf{H}_{\mathrm{STC}}$ are $\lambda_i^2 = |h_1|^2 + |h_2|^2 \pm 2|h_1 h_2| \sin(\Delta\theta)$ each λ_i^2 with multiplicity 2. Therefore, if the expected total power gain from the MISO configuration is preserved (i.e. $\mathrm{Tr}\left(\mathbf{H}_{\mathrm{STC}}^{\dagger}\mathbf{H}_{\mathrm{STC}}\right) = \sum_i \lambda_i^2 = 4(|h_1|^2 + |h_2|^2)$, where $\mathrm{Tr}(.)$ denotes the trace), the per-polarization, per-time-slot power gain and thus the condition number $\kappa = \max_i \lambda_i / \min_i \lambda_i$ depend on $\Delta\theta$. Equal power gain is achieved when the channel is perfectly conditioned ($\kappa = 1$), which in this model occurs when $\sin(\Delta\theta) = 0$, meaning the two transmit SOPs are aligned ($\theta_1 = \theta_2$) or anti-aligned ($\theta_1 = \theta_2 + \pi$). This dependence on $\Delta\theta$ also appears in decoding using $\mathbf{H}_{\mathrm{STC}}^{\dagger}$ (i.e. $\mathbf{H}_{\mathrm{STC}}^{\dagger}\mathbf{r}'_{\mathrm{STC}}$):

$$\begin{cases} \begin{pmatrix} \tilde{s}_X[k] \\ \tilde{s}_Y[k] \end{pmatrix} = (|h_1|^2 + |h_2|^2) \begin{pmatrix} s_X[k] \\ s_Y[k] \end{pmatrix} + \\ \qquad \mathbf{A} \begin{pmatrix} s_X[k+1] \\ s_Y[k+1] \end{pmatrix} + \begin{pmatrix} \bar{n}_X[k] \\ \bar{n}_Y[k] \end{pmatrix} \\ \begin{pmatrix} \tilde{s}_X[k+1] \\ \tilde{s}_Y[k+1] \end{pmatrix} = (|h_1|^2 + |h_2|^2) \begin{pmatrix} s_X[k+1] \\ s_Y[k+1] \end{pmatrix} + \\ \qquad \mathbf{A}^{\dagger} \begin{pmatrix} s_X[k] \\ s_Y[k] \end{pmatrix} + \begin{pmatrix} \bar{n}_X[k+1] \\ \bar{n}_Y[k+1] \end{pmatrix} \end{cases}$$

Because of the off-diagonal block in (8), the orthogonality of the STC scheme is lost when $\sin(\Delta\theta) \neq 0$ ($\mathbf{H}_{\mathrm{STC}}$ is ill conditioned), leading to inter-timeslot interference between consecutive symbols on both receive polarizations. To achieve the classical Alamouti power gain of $|h_1|^2 + |h_2|^2$ per-polarization and per-time-slot, the condition $\sin(\Delta\theta) = 0$ must be satisfied. The same sensitivity arises in the SPC configuration.Therefore, aligning the SOP between the two transmit branches appears to be critical to enable correct per-polarization decoding. Several solutions can be used to deal with this limitation such as using polarization-maintaining fiber (PMF) at the transmitter chains. It is assumed in the following of the paper that such control is applied to the transmit optical fields. Under this additional assumption and in the presence of Rx SOP rotation only, the STC received signal becomes:

$$\begin{aligned}\mathbf{r}_{\mathrm{STC}} = \mathbf{R}_{\alpha_{Rx}} \Bigg(h_1 \begin{pmatrix} s_X[k] & -s_X^*[k+1] \\ s_Y[k] & -s_Y^*[k+1] \end{pmatrix} + \\ h_2 \begin{pmatrix} s_X[k+1] & s_X^*[k] \\ s_Y[k+1] & s_Y^*[k] \end{pmatrix} \Bigg) + \begin{pmatrix} n_X[k] & n_X[k+1] \\ n_Y[k] & n_Y[k+1] \end{pmatrix}\end{aligned}$$

The receive SOP rotation can be compensated using data-aided techniques. After SOP rotation compensation, decoding is enabled to recover the transmitted symbols correctly just as in the SISO case.

The instantaneous post-combining signal-to-noise ratio (SNR) per recovered symbol per polarization can be deduced from decoding (3) and (5) is the same and it can be expressed as follows:

$$\mathrm{SNR}_{\mathrm{inst}} = (|h_1|^2 + |h_2|^2)\, \mathrm{SNR}_{\mathrm{static}}$$

where $\mathrm{SNR}_{\mathrm{static}}$ is the per-polarization SNR determined by the static received optical power (ROP). This expression depends only on channel amplitudes since the phases are canceled with Alamouti decoding. Consequently, for performance evaluation we use amplitude time-series only.

IV. Realistic Atmospheric Turbulence Time-Series

A. Time-Series Parameters

Thales Alenia Space derives the performance evaluation of the SISO and MISO systems based on advanced time series produced by a sophisticated, field-validated simulator also

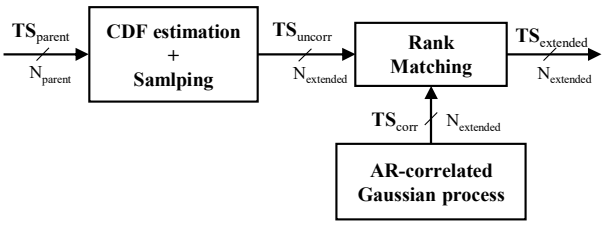

Fig. 7. Rank Matching method

used in the system design. These time-series represent realistic GEO conditions, including AO correction and dynamically varying turbulent channel. Two distinct scenarios are considered, 20 cm LO-AO (*Low Order – Adaptive Optics*) and 50 cm (*High Order – Adaptive Optics*), differing mainly by the transmitter aperture diameter; all other parameters are identical which allows isolating transmit aperture size and AO effects (Table I).

TABLE I. TIME-SERIES UPLINK SCENARIOS

Parameter	***Scenario 20 cm LO-AO***	***Scenario 50 cm HO-AO***
D_{Tx} (cm)	20	50
D_{Rx} (cm)	30	30
Elevation (°)	30	30
r_0 (cm)	5.11	5.11
AO radial orders	4	12
F_s (KHz)	4	4

For each scenario, only a 10-second snapshot is available, with 4×10^4 realizations, recorded at a sampling frequency of 4 KHz. These records represent realistic fluctuations, but their total duration and number of samples are not sufficient for statistically robust performance analysis. We therefore extend the duration of the available time-series data by generating new samples with the same distribution and correlation properties. The extension method and its validation are described next.

B. Extension of the time-series

To extend the parent (original) time series $\mathbf{TS}_{parent}$ while preserving the first- and second-order statistics, we use the method Rank Matching [20]. This method was initially proposed to generate synthetic correlated Gamma-Gamma fluctuations to model an FSO channel with prescribed correlation properties. The diagram in Fig. 5 describes the method used. It consists of three steps:

- **Uncorrelated time-series generation:** in this step, we generate uncorrelated time-series $\mathbf{TS}_{uncorr}$ of $N_{extended}$ samples that have the same statistical distribution as the parent time-series $\mathbf{TS}_{parent}$ of N_{parent} ($<< N_{extended}$) samples. To do so, the cumulative distribution function (CDF) of $\mathbf{TS}_{parent}$ is estimated. This estimated CDF is then used to generate i.i.d new samples using inverse transform sampling which relies on the empirical inverse of the CDF.
- **Correlated Gaussian samples generation:** the autoregressive (AR) model [21] is used to generate $N_{extended}$ correlated Gaussian samples $\mathbf{TS}_{corr}$ that have approximately the same empirical auto-correlation function (ACF) as the parent time-series.

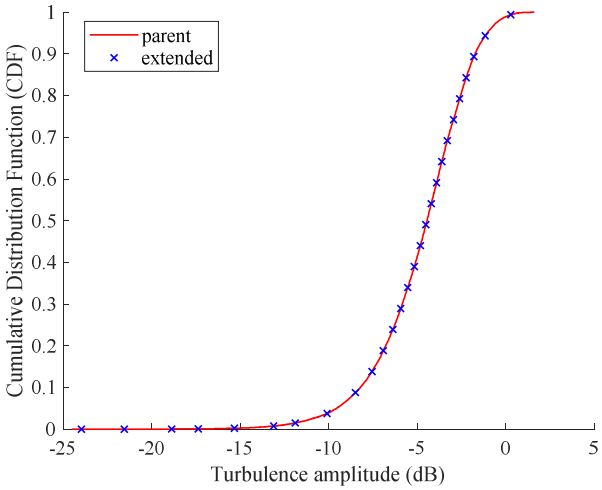

Fig. 5. Empirical CDF of TS_{par} in dB of Scenario 20 cm LO-AO: parent ($N_{parent} = 4\times10^4$) vs extended ($N_{extended} = 5\times10^6$)

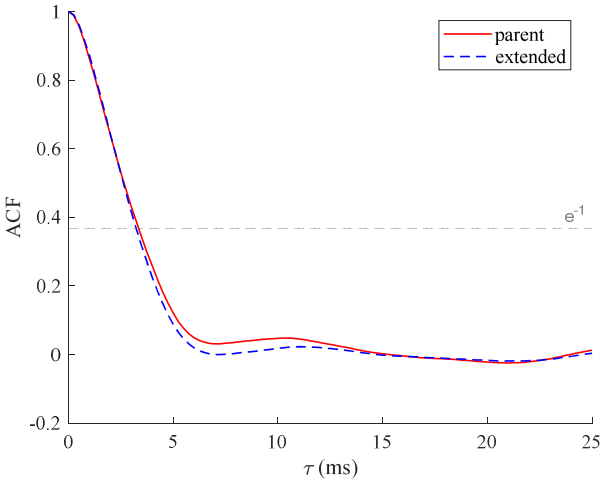

Fig. 6. Empirical ACF vs lag (ms) of Scenario 20 cm LO-AO: parent ($N_{parent} = 4\times10^4$) vs extended ($N_{extended} = 5\times10^6$)

- **Rank Matching:** As detailed in [22], this method reorders the uncorrelated time-series $\mathbf{TS}_{uncorr}$ according to the rank order of the sorted correlated Gaussian samples $\mathbf{TS}_{corr}$ to match the desired autocorrelation of the parent time-series $\mathbf{TS}_{parent}$, so the resulting $\mathbf{TS}_{extended}$ preserves the statistical distribution and the correlation properties of $\mathbf{TS}_{parent}$.

We validate the method comparing the empirical CDF and the empirical ACF of parent and extended time-series. Representative results for *Scenario 20 cm LO-AO* are shown in Fig. 6 and Fig. 7: an extended sequence of $N_{extended} = 5\times10^6$ generated from parent data of length $N_{parent} = 4\times10^4$. The extension applied to *Scenario 50 cm LO-AO* shows equivalent agreement.

For a deeper validation, we also compared the following fade statistics [15]:

- **Level Crossing Rate (LCR)**: LCR at a given threshold is the average number of upward (or downward) crossings per second. In this comparison, we report up-crossings as performed in [15]. The extended series reproduces the LCR curve of the parent data over a representative range of threshold, as the parent time series is too short to estimate the full curve reliably (Fig. 8).

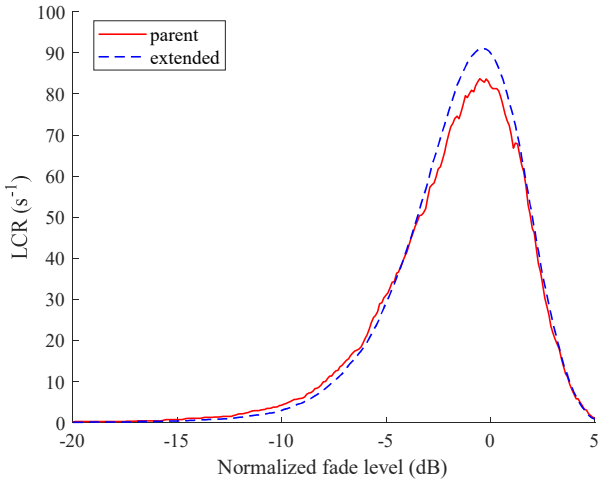

Fig. 8. Level Crossing Rate (LCR) vs normalized fade level (dB) of Scenario 20 cm LO-AO: parent ($N_{parent} = 4\times10^4$) vs extended ($N_{extended} = 5\times10^6$)

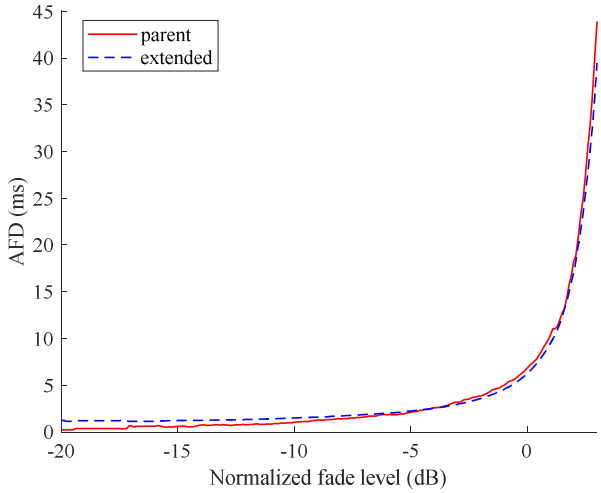

Fig. 9. Average Fade Duration (AFD) vs normalized fade level (dB) of Scenario 20 cm LO-AO: parent ($N_{parent} = 4\times10^4$) vs extended ($N_{extended} = 5\times10^6$)

- **Average Fade Durations (AFD)**: AFD at a given threshold is the average time during which the process remains below the threshold during a fade event. Empirically, AFD is obtained by detecting all fade intervals where the process is below the threshold, then averaging their durations. Fig. 9 shows close agreement between parent and extended AFD curves over a representative range of thresholds as done for LCR.

The x-axis of Fig. 8 and Fig. 9 represents the normalized fade level in dB, computed as follows (where E(.) denotes the average value):

$$\text{Normalized fade level} = \text{threshold} - 10\log_{10}(E(\mathbf{TS}))$$

These validations indicate that the Rank Matching approach, combined with AR based correlation synthesis, produces extended time-series that are statistically similar to the original data. Consequently, the generated time-series are suitable for evaluating SISO and MISO links under realistic GEO turbulence and AO conditions.

V. Simulation Results and Discussion

This section presents a high-level performance comparison between SISO and MISO systems. We report numerical results for both systems and discuss the trade-offs revealed by the simulation results.

A. System parameters and performance metric

To compare the performance of the MISO (STC/SPC) and the SISO systems, the per-polarization Received Optical Power (ROP) in dBm is taken from a representative Thales Alenia Space link budget. The static ROP includes all component and propagation static gains and losses:

- **Scenario 20 cm LO-AO**: transmit diameter D_{Tx} = 20 cm results in ROP_{static} = -41 dBm.
- **Scenario 50 cm HO-AO**: transmit diameter D_{Tx} = 50 cm results in ROP_{static} = -33 dBm.

Per-polarization static SNR in dB is derived from ROP using the following equation:

$$\text{SNR} = -10\log_{10}(hf\text{R}_s) - \text{NF} + \text{ROP}$$

where h is the Planck's constant, f is the optical carrier frequency at 1550 nm, NF is the receiver noise figure, and R_s = 56 GBd is the per-polarization symbol rate.

Since the FSO turbulent channel is a block fading channel, the performance metric used is the outage probability $P_{out} = Pr(MI < R_0)$ where MI is the per-polarization constrained MI of Gray-mapped QPSK as a function of instantaneous SNR $MI(SNR_{inst}) \in [0, 2]$ bits/symbol. $R_0 \in [0, 2]$ bits/symbol is the per-polarization target rate, with $R_0 = 2R_c$ for QPSK modulation and $0 < R_c < 1$ is the FEC code rate.

Interleaving is emulated by averaging MI over a moving time window of duration T_{int}. Outage is evaluated as a function of interleaving depth (T_{int}) and target rate (R_0). The outage probability is the fraction of samples with $MI < R_0$. We present results at $P_{out} = 10^{-3}$ (99.9% availability), which is a commonly used target availability in Very High Throughput Systems (VHTS) [23].

B. Performance comparison and discussions

1) Compared configurations and results

We compare three MISO configurations against a SISO *50 cm HO-AO* reference configurations under two transmit power levels: Power-constrained (PC) that conserves total transmitted optical power by splitting it equally across the MISO apertures (-3 dB per aperture relative to SISO), and Power-augmented (PA) that assigns each MISO aperture the same power as SISO, doubling total transmit power (+3 dB). The three MISO configurations are:

- ***Baseline* (PC-2×50-HOAO):** power-constrained with two 50 cm apertures and high order AO.
- ***Cost-optimized* (PC-2×20-LOAO):** power-constrained with two 20 cm apertures and low order AO.
- ***Intermediate* (PA-2×20-LOAO):** power-augmented with two 20 cm apertures and low order AO.

The *Baseline* configuration duplicates the reference SISO system's aperture and AO quality while keeping the total transmit power unchanged. The *Cost-optimized* configuration reduces aperture size and AO radial orders while maintaining the same total transmit power as SISO. The *Intermediate* configuration retains the small apertures and low-order AO

of the *Cost-optimized* design while allocating the SISO transmit power to each aperture. We refer to it as *Intermediate* because, by construction, it lies between the *Baseline* and *Cost-optimized* configurations in terms of apertures/AO complexity and power allocation.

TABLE II. COMPARATIVE ANALYSIS OF KEY SYSTEM METRICS FOR THE THREE MISO CONFIGURATIONS AT $P_{OUT} = 10^{-3}$

Gains vs SISO	***Baseline***	***Cost-optimized***	***Intermediate***
Per-aperture Tx power[a]	-3 dB	-3 dB	0 dB
Achievable rate at $T_{int} = 50$ ms[b]	+ 46.2%	+ 5.5%	+ 53.4%
Interleaver depth T_{int} at $R_0 = 1$ bit/symbol[a]	- 67.4%	+ 22.6%	-85.6%
Total aperture area[a]	× 2	÷ 3.125	÷ 3.125
Per-aperture AO radial orders[a]	× 1	÷ 3	÷ 3

[a.] lower is better
[b.] higher is better

Table II reports two classes of gains relative to the SISO configuration. By-design gains are fixed by hardware and power allocation choice such as the collecting aperture area, AO radial orders, and per-aperture transmit power and do no depend on the turbulent channel. Performance gains (as shown in Fig. 10) reflect link performance under the outage criterion $P_{out} = 10^{-3}$, such as the achievable rate at a fixed interleaver depth $T_{int} = 50$ ms and the interleaver depth required to meet a target spectral efficiency of 1 bit/symbol, corresponding to a code rate $R_c = 1/2$. This is one of the FEC rate specified in the CCSDS (Consultative Committee for Space Data Systems) Orange Book for High Data Optical Communications – 1550 nm. Because telescope gain scales with the collecting aperture area, we report gain in terms of area instead of diameter to ensure a fair, physically consistent comparison across configurations.

At $R_0 = 1$ bit/symbol, *Baseline* configuration reduces the required interleaver depth T_{int} by 67.4% relative to SISO, and at fixed interleaver depth $T_{int} = 50$ ms, the achievable rate increases by 46.2%. *Intermediate* configuration uses double transmit power and spatial diversity, yielding the deepest reduction in interleaver depth (-85.6%) and the largest rate gain at $T_{int} = 50$ ms (+53.4%). In contrast, at equal total power, *Cost-optimized* configuration gains are modest: T_{int} increases by 22.6% at the target rate 1 bit/symbol, and the achievable rate is raised by only 5.5% at $T_{int} = 50$ ms. As shown in Fig. 10, these results are sensitive to both the target code rate and the target interleaver depth. If lower rates are targeted (e.g., 1/4, 1/3, or 2/5 as specified in the CCSDS recommendations), the interleaver depth gains for the *Cost-optimized* configuration become more significant. Similarly, achievable rate increases are more significant at lower interleaver depths.

Across all cases, the *Intermediate* option enables a reduction in AO radial orders and aperture size, lowering AO complexity, and cost, whereas *Baseline* design retains high order AO with lower per-aperture power. The choice of the best configuration therefore depends on the system-level trade-offs, as discussed next.

2) System trade-offs and design implications

- **Power budget:** Under a fixed total transmit power budget, *Baseline* configuration converts larger collecting area into performance, at the cost of high-order AO. When power margin exists, *Intermediate* configuration leverages both diversity and added per-aperture to deliver the best performance (-85.6% reduction in T_{int} at 1 bit/symbol and 53.4% achievable rate raise at $T_{int} = 50$ ms) at the expense of higher electrical load in the Tx power chain, that may not enable dual-polarized amplification as in the baseline architecture.
- **Optics and AO complexity:** Moving from 50 cm to 20 cm apertures reduces collecting area 3.125 times, which weakens the received SNR. However, the smaller optics enable a significant reduction in AO radial orders, reducing AO complexity, mass, size and cost. Baseline configuration maintains high order AO to maximize the benefit of the larger optics; *Intermediate* and *Cost-optimized* configurations reduce AO order, which makes the system simpler.
- **Throughput-latency trade-off:** If the constraint is low latency or limited interleaver memory, the *Intermediate* configuration is the most favorable (-85.6% T_{int} at $R_0 = 1$ bit/symbol), with *Baseline* configuration also very effective (-67.4%). At fixed latency (e.g., $T_{int} = 50$ ms), *Intermediate* configuration delivers the largest rate gain (+53.4%) when power margin allows. Under strict total-power, *Baseline* configuration enables a substantial achievable rate gain (+46.2%).
- **Integration constraints:** Two 50 cm apertures introduce higher mass and cost. Two 20 cm telescopes ease mechanical integration, simplify alignment and are cheaper and lighter. *Intermediate* configuration introduces additional power-chain complexity (dual-branch amplification as in the SISO reference architecture) compared to *Cost-optimized*.

Overall, the *Baseline* configuration is the best solution achieving high throughput at fixed latency under strict total-power constraints. The *Intermediate* configuration is the suitable solution in the case of a power increased budget system constrained by latency/memory and compact-optics requirements. The *Cost-optimized* configuration is primarily competitive for FEC code rates below 1/2 (Fig. 10), where it delivers significant performance gains while meeting stringent cost, mass, size, and power-limited constraints.

In light of the SISO constraints discussed in Section II, this study shows that MISO 2×1 system can be tuned in terms

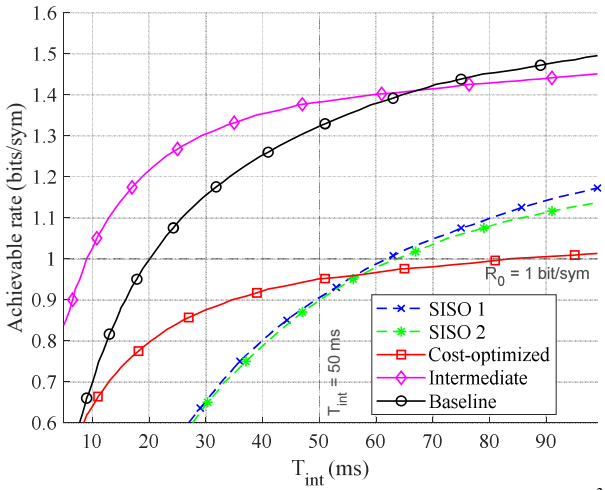

Fig. 10. Achievable rate vs interleaving depth T_{int} at $P_{out} = 10^{-3}$ for the reference SISO and the three MISO configurations

of aperture size along with AO radial orders, interleaving depth, and HPOA transmit power to meet the 99.9% availability target within realistic cost, weight, and memory constraints for ground-to-GEO FSO feeder links.

VI. Conclusion

This study presented a comparative analysis of three MISO configurations against a SISO large transmit aperture and high-order adaptive optics reference under two transmit power regimes: power-constrained and power-augmented. By evaluating key system metrics, such as achievable rate, required interleaver depth, aperture area, and AO complexity, we quantified the design trade-offs for each architecture. The *Baseline* configuration, using larger apertures and high-order AO with split transmit power, achieves significant gains over SISO under strict power limits. When additional system power is available, the *Intermediate* power-augmented MISO design produces the highest improvements in achievable rate and reduction in interleaver depth, while simplifying AO complexity and reducing aperture size. In contrast, the *Cost-optimized* solution, which uses smaller apertures and lower AO order while conserving power, enables a more compact, lighter, and cost-effective system, with smaller performance improvements.

Choosing the best configuration depends on the main system-level priorities, including available power, optical and AO complexity, throughput-latency balance, and integration requirements. Our findings show that MISO designs can be adapted to satisfy high availability (99.9%) for ground-to-GEO FSO feeder links, optimizing the mix of aperture size, AO complexity, interleaver depth, and transmit power within realistic cost, weight, and memory budgets.

The current analysis assumes ideal transmitter-side SOP rotation control and does not consider many practical polarization effects. In reality, polarization impairments can degrade decoding performance. Therefore, future studies should incorporate a more complete channel model that accounts for all relevant impairments, including atmospheric turbulence, as well as synchronization and hardware issues such as timing and frequency offsets, phase noise, and others. Additionally, exploring extended MISO architectures with more than two transmit apertures and advanced spatial encoding could further enhance performance and robustness for geostationary optical feeder uplinks.

Acknowledgment

This work was conducted in the framework of a PhD thesis co-funded by Thales Alenia Space and Région Bretagne.

References

[1] M. A. Khalighi and M. Uysal, "Survey on Free Space Optical Communication: A Communication Theory Perspective," IEEE Commun. Surveys Tuts., vol. 16, no. 4, pp. 2231–2258, 2014, doi: 10.1109/COMST.2014.2329501.

[2] H. Kaushal and G. Kaddoum, "Optical Communication in Space: Challenges and Mitigation Techniques," IEEE Commun. Surveys Tuts., vol. 19, no. 1, pp. 57–96, 2017, doi: 10.1109/COMST.2016.2603518.

[3] N. Maharjan, N. Devkota, and B. W. Kim, "Atmospheric Effects on Satellite–Ground Free Space Uplink and Downlink Optical Transmissions," Appl. Sci., vol. 12, 10944, 2022, doi: 10.3390/app122110944.

[4] H. Kotake et al., "First experimental demonstration of optical feeder link by using the optical data relay satellite LUCAS," Proc. SPIE, vol. 12777, Jul. 2023, doi: 10.1117/12.2689017.

[5] C. Petit et al., "Onera's optical ground station for Geo Feeder links FEELINGS: in lab testing and on sky implementation," in Proc. 2023 IEEE ICSOS, Vancouver, BC, Canada, 2023, pp. 193–197, doi: 10.1109/ICSOS59710.2023.10490280.

[6] Y. Horst, B. Bitachon, L. Kulmer et al., "Tbit/s line-rate satellite feeder links enabled by coherent modulation and full-adaptive optics," Light Sci. Appl., vol. 12, 153, 2023, doi: 10.1038/s41377-023-01201-7.

[7] M. Gregory, F. Heine, H. Kämpfner, R. Lange, K. Saucke, U. Sterr, R. Meyer, "Inter-satellite and satellite-ground laser communication links based on homodyne BPSK," Proc. SPIE, vol. 7587, Free-Space Laser Commun. Technol. XXII, 75870E, Feb. 2010, doi: 10.1117/12.847888.

[8] S. M. Alamouti, "A simple transmit diversity technique for wireless communications," IEEE J. Sel. Areas Commun., vol. 16, no. 8, pp. 1451–1458, Oct. 1998, doi: 10.1109/49.730453.

[9] P. Hanne et al., "Real-Time 10 Gbit/s Digital Combining Over a 3 km Free-Space Optical Link With Multi-Aperture Receiver," in Photonic Networks: Proc. 24th ITG Symp., Berlin, 2023, pp. 1–4.

[10] M.-C. Cheng et al., "1-Tb/s/3.9-km FSO Propagations With WDM-PAM4 Technique and Telescope-Type Four-Lens System," J. Lightwave Technol., vol. 43, no. 17, pp. 8215–8224, Sept. 2025, doi: 10.1109/JLT.2025.3584586.

[11] K. Matsuda et al., "Demonstration of a Real-Time 14 Tb/s Multi-Aperture Transmit Single-Aperture Receive FSO System With Class 1 Eye-Safe Transmit Intensity," J. Lightwave Technol., vol. 40, no. 5, pp. 1494–1501, Mar. 2022, doi: 10.1109/JLT.2021.3132306.

[12] D. J. Geisler, T. M. Yarnall, C. M. Schieler, M. L. Stevens, and B. S. Robinson, S. A. Hamilton, "Experimental demonstration of multi-aperture digital coherent combining over a 3.2-km free-space link," Proc. SPIE, vol. 10096, Free-Space Laser Commun. Atmos. Propag. XXIX, 100960C, Feb. 2017, doi: 10.1117/12.2256581.

[13] A. Le Kernec et al., "The H2020 VERTIGO project towards tbit/s optical feeder links," Proc. SPIE, vol. 11852, Int. Conf. Space Opt. ICSO 2020, 1185217, Jun. 2021, doi: 10.1117/12.2599229.

[14] D. R. Arrieta et al., "Proof-of-Concept Real-Time Implementation of Interleavers for Optical Satellite Links," J. Lightwave Technol., vol. 41, no. 12, pp. 3932–3942, Jun. 2023, doi: 10.1109/JLT.2023.3270769.

[15] H. D. Le and A. T. Pham, "Level Crossing Rate and Average Fade Duration of Satellite-to-UAV FSO Channels," IEEE Photonics J., vol. 13, no. 1, pp. 1–14, Feb. 2021, Art. no. 7901514, doi: 10.1109/JPHOT.2021.3057198.

[16] J. Zhang, S. Ding, H. Zhai, and A. Dang, "Theoretical and experimental studies of polarization fluctuations over atmospheric turbulent channels for wireless optical communication systems," Opt. Express, vol. 22, pp. 32482–32488, 2014.

[17] J. P. Palastro, "Time-dependent polarization states of high-power, ultrashort laser pulses during atmospheric propagation," Phys. Rev. A, vol. 89, no. 1, p. 013804, Jan. 2014, doi: 10.1103/PhysRevA.89.013804.

[18] M. S. Faruk and S. J. Savory, "Digital Signal Processing for Coherent Transceivers Employing Multilevel Formats," J. Light. Technol., vol. 35, no. 5, pp. 1125–1141, Mar. 2017, doi: 10.1109/JLT.2017.2662319.

[19] D. Tse and P. Viswanath, Fundamentals of Wireless Communication. Cambridge, U.K.: Cambridge University Press, 2005.

[20] G. T. Djordjevic, P. Ivanis, J. Makal, D. Milic, and V. Kafedziski, "A Method for Generating Random Process Having Given First- and Second-Order Statistics Over FSO Channel," 2024 14th Int. Symp. Commun. Syst., Netw. Digit. Signal Process. (CSNDSP), Rome, Italy, 2024, pp. 7–11, doi: 10.1109/CSNDSP60683.2024.10636442.

[21] K. E. Baddour and N. C. Beaulieu, "Autoregressive modeling for fading channel simulation," IEEE Trans. Wireless Commun., vol. 4, no. 4, pp. 1650–1662, Jul. 2005, doi: 10.1109/TWC.2005.850327.

[22] J. C. Silveira Santos Filho, M. D. Yacoub, and G. Fraidenraich, "A simple accurate method for generating autocorrelated Nakagami-m envelope sequences," IEEE Commun. Lett., vol. 11, pp. 231–233, Mar. 2007.

[23] L. Canuet, "Coherent optical feeder links for very high throughput satellite systems," Proc. SPIE, vol. 12877, Free-Space Laser Commun. XXXVI, 128770E, Mar. 2024, doi: 10.1117/12.3002913.